Additive Manufacturing 24 (2018) 125–136

Contents lists available at ScienceDirect

Additive Manufacturing

journal homepage: www.elsevier.com/locate/addma

Standardized X-ray tomography testing of additively manufactured parts: A round robin test

Anton du Plessis[a,b,*], Stephan G. le Roux[b]

[a] Physics Department, Stellenbosch University, Stellenbosch, 7602 South Africa
[b] CT Scanner Facility, Stellenbosch University, Stellenbosch, 7602 South Africa

ARTICLE INFO

Keywords:
X-ray tomography
microCT
Additive manufacturing
Laser powder bed fusion
Ti6Al4V

ABSTRACT

Micro computed tomography (microCT) allows non-destructive insights into the quality of additively manufactured parts and the processes that produce them. MicroCT has been used widely in this industry but the use of this technique is often time consuming and costly which reduces its potential impact and the benefits associated with its use. By using standardized test procedures, the analysis time and cost can be minimized and confidence in obtained results increased. A round robin test was conducted as follows: a series of standard test procedures (part sizes and shapes and test protocols) were applied – using one microCT system – to identical parts produced on a variety of metal additive manufacturing systems (specifically laser powder bed fusion systems). These are simple parts: a 10 mm cube, a 15 mm diameter vertical-built cylinder and a basic topology optimized example part – a bracket. The 15 mm diameter cylinder acts as witness specimen for the build of the complex part. All these were produced in Ti6Al4V, and in some cases parts were provided with variations in process parameters or manufacturing conditions which led to different types of intentional manufacturing flaws or defects. Various intentional and unintentional flaws were identified and quantified. The major result shown is that the analysis of a simple 10 mm cube clearly identifies incorrect process parameters even for very low levels of porosity, with unique porosity distributions and characteristics. It is found that generally this porosity extends to larger, more complex parts. The witness specimen (15 mm cylinder) allows clear identification of layered stop-start flaws, at a resolution better than a complex part built alongside it, allowing to identify defective builds. The results indicate a successful first step at standardized microCT analysis procedures for improvement of processes and quality control in additive manufacturing.

1. Introduction

Additive manufacturing (AM) is fast growingas a method to produce custom, complex and lightweight parts for industrial applications [1]. A major industrial interest is the production of metal parts which is possible in various metal alloys with excellent mechanical properties including in Ti6Al4V [2,3]. Laser powder bed fusion allows the manufacturing of relatively large parts with intricate, complex designs with minimal post-processing required, compared to other metal AM methods. These type of parts have particular benefits for applications in aerospace and medical fields, since lightweight parts can be produced using topology optimized and latticed designs. For Ti6Al4V mechanical performance of AM parts can be superior to traditionally manufactured equivalents [4]. However, despite the huge potential of the technique, some consistency problems remain. Most importantly, manufacturing flaws can occur due to various physical problems such as insufficient laser power, insufficient track overlap and uneven powder spreading, amongst many others. Due to the complex nature of the additive manufacturing workflow, quality control and testing is necessary at various steps in the process to ensure consistently high density parts with good mechanical properties, good geometric tolerances and lack of residual stresses [5]. Standardization of additive manufacturing testing workflows provide one step towards the improvement of the quality of produced parts as described in [6].

Non-destructive testing of AM parts using a variety of tools was discussed in [7] and in a careful study with samples of varying levels of porosity in [8]. Micro computed tomography (microCT) in particular has been used with great success in the field of AM and new capabilities and accessibility of the technique continue to expand its wider use as discussed in a recent review paper [9]. This review paper highlights many examples of its use for dimensional analysis, porosity analysis and many more newer analysis methods such as lattice structure

* Corresponding author.
E-mail address: anton2@sun.ac.za (A. du Plessis).

https://doi.org/10.1016/j.addma.2018.09.014
Received 3 August 2018; Received in revised form 5 September 2018; Accepted 11 September 2018
Available online 20 September 2018

characterization, surface roughness measurement and more, especially in metal laser powder bed fusion. Its use for other 3D printing characterization is also widespread as evidenced by examples of its use in characterization of parts produced in plastic extrusion printing [10], plastic 3D printer filament characterization [11], characterization of carbon and glass fibre reinforced plastics [12] and even for characterization of 3D printed electronic devices [13].

MicroCT is often used to analyse produced parts for internal porosity, cracks, or geometric deviations from design, on a part-by-part quality inspection basis. This is useful for critical parts such as those in medical and aerospace industries, to ensure lack of major flaws or irregularities. Another powerful but hugely under-utilized application thus far is to use microCT to improve process parameters and better understand the effect of parameters on the obtained microporosity. In both of the above cases however, there are major differences between scans depending on the multitude of scan parameters that can be selected, part sizes and hence resolution obtained and image analysis and data analysis options. This results in misinterpretation of microCT results, or non-acceptance of these results. In earlier work, quality control was demonstrated with a reference sample to validate the ability to detect small pores in a specific scan using a cast metal part as reference due to its smaller pores than the additive part [14]. However, best possible scan quality is obtained with individual parts and reference parts with pores might not be available everywhere or have the same dimensions.

Some developments towards producing standards for microCT testing of AM parts are ongoing [15–17]. In the interests of further standardization and quantitative analysis for AM using microCT, a series of simplified methods were recently developed based on standard microCT tests which can be applied to Ti6Al4V parts. These include the production of a 10 mm cube coupon sample, scanned at 15 µm voxel size using pre-determined voltage and current and other settings possible on most typically available laboratory microCT systems. This 10 mm cube sample data is then analyzed according to a fixed methodology (recipe) to allow quantitative analysis of cube porosity [18], mean density [19] and surface roughness [20]. This information can be used to analyse the process parameters and potentially optimize and improve the manufacturing process, or can be used as a start point for analysis of quality issues in the production workflow.

For quality inspections, a witness specimen (15 mm diameter cylinder) has been suggested for production together with a critical/complex part (alongside it in the same build), which can be analysed at higher resolution than the complex part using microCT [6]. In this previous work it was shown for one case that the porosity distribution did not transfer/correlate directly with the witness specimen. This is to be expected as thermal gradients and scan tracks vary with complex shapes of the part. Nevertheless, the witness specimen (which is a 15 mm diameter cylinder built vertically) may be analysed at a higher resolution in a standardized method as described in [21], including standardized scan parameters due to the sample width remaining constant. This provides an insight into possible major layered flaws such as stop-start flaws which might have occurred during the build process. The powder feedstock used in the process may also be analysed by microCT scanning. This can be done to visually check for possible contamination (denser or less dense particles seen in CT images), for large amounts of porosity in powder particles or to check for highly irregular-shaped particles. Besides qualitative checks, quantitative analyses are also possible as described in more detail in a standardized workflow for this sample type presented in [22].

The methods described above aim to improve confidence in microCT results through fixed settings and analysis procedures, removing human bias in the process as far as possible. The use of microCT for these analyses have been demonstrated by many authors, but this work aims to standardize this process for routine use in quality control. The use of microCT in additive manufacturing is reviewed in detail in [9], and is widely used for analysis of metal additively manufactured parts using both lab-based CT systems and synchrotron tomography. These analyses are typically for porosity or dimensional analyses. Measurement of surface roughness of parts is a relatively new capability which has recently been demonstrated in [23–26] and powder analysis is also a relatively new capability demonstrated recently by some authors [27–29].

Fig. 1. A typical set of Ti6Al4V parts produced in this round robin test: a 10 mm cube, a 15 mm diameter witness specimen rod and a complex shaped bracket (STL file in supplementary material).

Table 1
Basic microCT scan settings.

	Cube	Witness rod	Bracket
Voltage	200 kV	200 kV	200 kV
Current	50 µA	50 µA	120 µA
Voxel size	15 µm	25 µm	45 µm

Despite its increasing use and huge potential benefit to the additive manufacturing community, microCT has some inherent limitations. The first is the time duration of the scanning and image analysis procedure, which affects the cost and the throughput of parts. By using faster scanning options, the ability to detect small defects is compromised. However, excessive scan times are not practical, making its use still often only exploratory. Related to the scan time, is the possibility for the presence of image artefacts, which degrade image quality and may result in lack of results from a scan or require scan parameter modifications, adding further time and cost. The most important image artefacts are beam hardening, cupping and cone beam artefacts. These and other limitations on part size and resolution are described in more detail in [30]. The second major limitation is lack of standards or knowledge of the technique, i.e. it is not a routine method yet. This round robin test aims to provide a first step to address the above issues.

In this paper we report on the results of a comprehensive round robin test whereby the above developed standardized methods were applied to a series of parts produced at different facilities. In this work, identical Ti6Al4V samples were produced on a series of different AM systems (laser powder bed fusion in particular) from a variety of sources including academia and industry, from facilities on three continents. Due to the many potential causes of flaws and build imperfections, the specific participants are not named in this paper. The aim here is to highlight the typical types of defects and irregularities that can be identified with these standardized methods, how these correlate from

Table 2
Summary of parts produced and quick description of results of each. Each number corresponds to a different participant that produced a set of parts.

Sample Name	Comment	Results found
1a	Powder scraper not ideal (intentional)	Good density, some surface defects (notches)
1b	Layered stop-start flaw induced (intentional)	Good density, some surface defects, layered flaw found in witness specimen but not in bracket
2a	Good part attempted	Porosity low levels evenly distributed
2b	Contour scan track spacing increased (intentional)	Higher porosity
2c	Hatch spacing increased (intentional)	Highest porosity
3	Good part attempted	Contour pores found along vertical walls, warping found up to 1 mm on each vertical part of bracket
4	Good part attempted	Excellent surface finish and mean density, subsurface porosity found along top-facing surfaces
5	Good part attempted	Excellent density, contamination identified

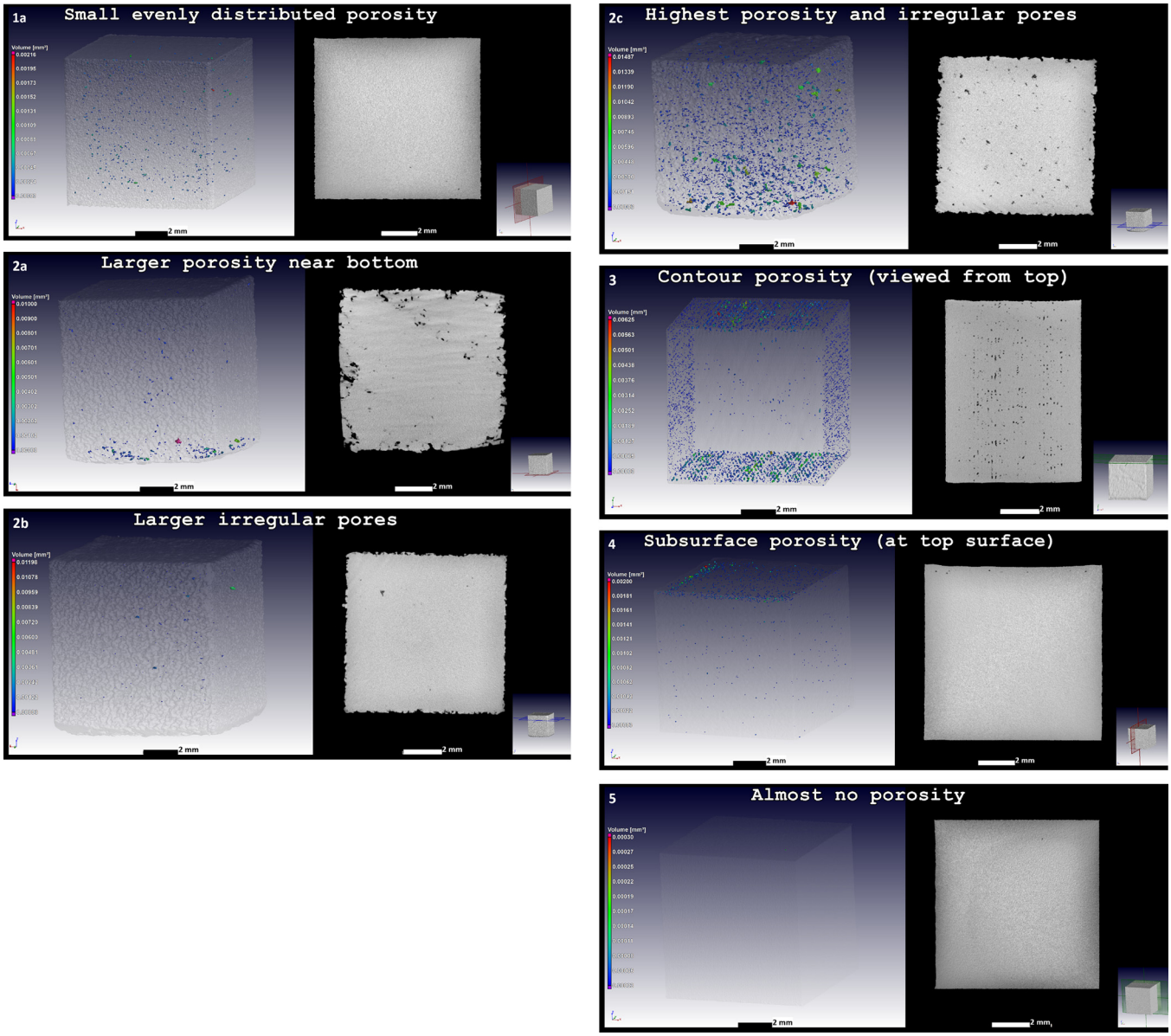

Fig. 2. Cube porosity images for each sample – colour scale varies according to the data set in each case (sample number indicated in each case). Note the different porosity distributions in 3D. Supplementary 3D rotation videos are provided for each cube.

cube to complex part, how a layered defect can be detected in the witness specimen and how both intentional and unintentional flaws are detected. The wealth of information from this round robin test is expected to contribute to the wider adoption of these methods for the improvement of the quality of AM parts, also with slight modifications for other materials.

2. Materials and methods

Each participant in this round robin study (being a producer of metal AM parts) was asked to manufacture and submit the following Ti6Al4V parts for testing:

- **One 10 mm cube**, built square without supports and cut from the

Table 3
Summary of cube porosity analysis.

Sample Name	Cube porosity (%)	Largest pore (mm)	Number of pores	Comment
1a	0.003	0.19	442	Evenly distributed porosity, rough surface with potentially closed pores not included
1b				N/A due to non-submission of cube
2a	0.012	0.76	355	Porosity mostly around edges indicating contour scan track error – not enough overlap of internal hatch tracks and contour tracks in scan strategy
2b	0.031	0.58	964	Also mostly contour porosity
2c	0.129	0.91	4080	Lack of fusion with significant amount of porosity
3	0.082	0.58	5628	Very strong contouring error – most pores along vertical walls
4	0.017	0.19	1137	Subsurface pores under top surface – spherical and numerous
5	0.000029	0.052	2	Very small porosity, but significant amount of dense inclusions found.

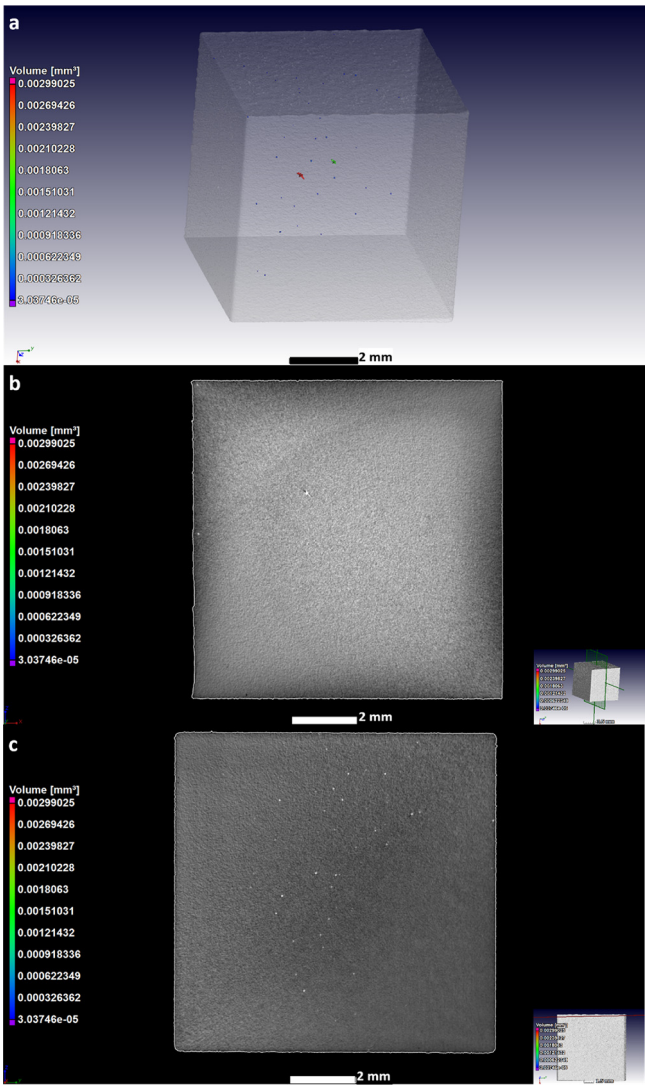

Fig. 3. Inclusions in one cube sample (sample number 5) shown in colour in 3D and as bright white dots in the slice images.

base (only cut one side)

- **A complex bracket which was provided as STL file**: built in the "base-down" orientation so as to minimize the use of support structures. This was a relatively small part, with approx. dimensional envelope of 60 mm × 40 × 40 mm. The STL file of this bracket is attached as supplementary material.
- **A witness specimen**: a 15 mm cylinder built vertically in the same build as the complex bracket, covering the entire height of the sample, i.e. it was approx. 40 mm high in this case.

Table 4
Summary of cube density values.

Sample Name	CT Density g/cm^3
1a	4.502
1b	N/A
2a	4.495
2b	4.488
2c	4.467
3	4.493
4	4.467
5	4.431

It was suggested that all parts be subjected to standard stress-relief heat treatment, supports removed and the sample cut from the base, with no further post processing. A representative set of parts is shown in Fig. 1. The bracket was designed as part of another project which is not further discussed here, and was designed using topology optimization software (Altair Inspire).

MicroCT scanning was performed according to the newly proposed standardized methods described in more detail in [18–22], and also available freely on protocols.io. These standardized methods are aimed at reproducibility in reporting of microCT results in the AM community, and is a suggested workflow with standard sample sizes which allows almost identical scan settings on different microCT systems and minimizes user influence in image analysis workflow (much of the process is automated). In addition to reproducibility, the methods are simplified, use commercially available software tools and are aimed at fast throughput (scan plus analysis should be 2 h for each part). The methods are described in this section but more details are found in the aforementioned references. A typical laboratory microCT system was used [30,31] with settings as in the Table 1 below and beam filtration using 0.5 mm copper. All image analysis was performed with Volume Graphics VGSTUDIO MAX 3.2.

The first three methods make use of the 10 mm cube sample and involves the same scan data, to extract information on porosity, mean density and surface roughness. This sample size allows a reasonably high resolution for microCT while still being representative for typical additive manufacturing processes. This sample is loaded at an angle (not critical but roughly 30–45°) and scanned at 15 µm voxel size using high quality settings which allows total scan time of approximately 1 h. Specifically in this case a General Electric Vtomex L240 system was used, with a reflection-target X-ray source with Tungsten target, 0.5 mm copper beam filtration, focus-to-detector distance was set to 600 mm, flat-panel detector pixel size was 200 µm and no binning was used. Images were acquired with 500 ms per image, averaging of 2 images at each step position and skipping of the first image at each step position, in a total of 2400 steps in a full rotation of the sample. Reconstruction was performed in system-supplied Datos software which includes strong beam hardening correction (value 9 in this software) to ensure no cupping artefacts are present. Automatic scan optimizer function was applied to find the accurate rotation axis value for sharp images in reconstruction.

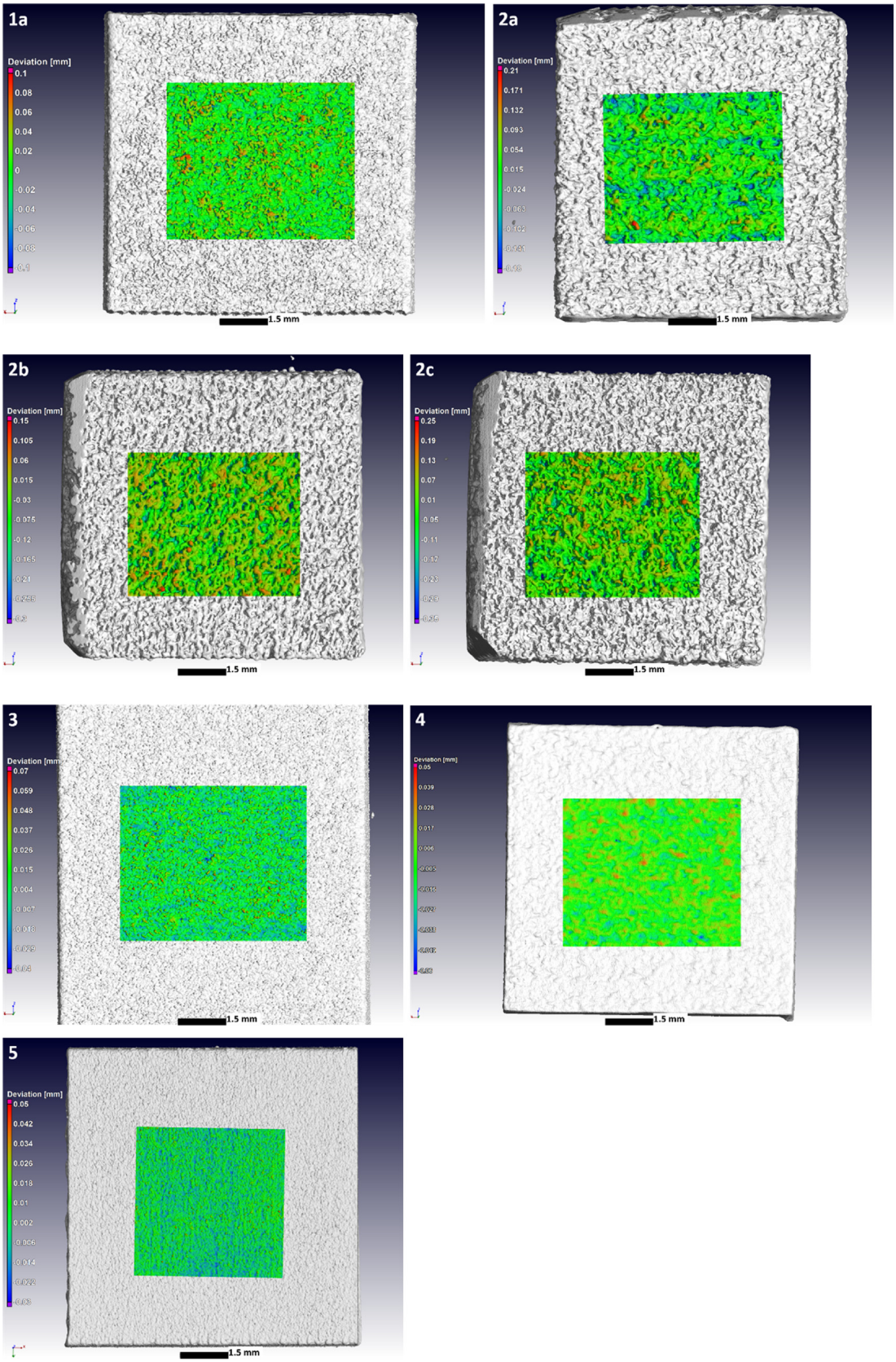

Fig. 4. Surface roughness measurements from all cube samples with sample numbers indicated, individual colour coding was applied to each data set.

Table 5
Summary of cube surface roughness results.

Sample Name	CT-derived S_a value (μm)
1a	18
1b	–
2a	35
2b	59
2c	59
3	10
4	8
5	5

The analysis of the cube data for porosity involves selection of the cube edge as a region of interest (ROI), ensuring that no external particles are included in the selection. The cube ROI is selected in such a way to include all internal pores/voids. The ROI selection is eroded by two voxels to remove the first two layers of voxels around the edge, to minimize possible edge errors. This new "internal" ROI is extracted. Up to this point every step is automated and no human bias can affect the measurement. This new internal volume is used as a basis for a new segmentation of pore spaces: a locally optimized (advanced function) surface determination is applied to the pore space/material threshold by human selection of the air and material peaks in the histogram and selecting the midpoint. If no clear peak is seen in the histogram due to low quantities of pores, the threshold is selected to the left of the material peak, with some input from visually checking the slice images and the local optimization applied in the same way. A new ROI is selected from this pore space segmentation and a defect analysis function applied using the "custom defect mask" method, thereby not using any special algorithm – all selected pores are classified and summed to provide the porosity total, maximum pore size and number of pores.

The analysis of the cube data for mean density is relatively simple is an accurate surface determination of the cube was applied in the previous step – once the edge of the cube is accurately determined and all internal pores are included, the total volume is easily obtained. This CT volume combined with a scale mass of the cube to provide a mean density value.

The analysis of the cube data for surface roughness also uses the surface determination applied in the previous step, but a local region of interest where the analysis is applied is selected, extracted and a new surface determination obtained to ensure highest possible quality locally optimized thresholded edge data (with sub-voxel precision possible with high quality data). This surface topography is compared to a mean surface of the same region in a nominal-actual comparison for effectively a surface topography colour-map. Variances are extracted in excel and calculation of mean S_a value is possible over the ROI.

The analysis of the complex part cannot entirely be fixed as complex parts may vary in size or complexity, affecting scan parameters. Therefore the scans of the complex parts were done using typical high quality settings to check for major flaws and, in this study, to correlate porosity of cubes with those in the brackets. The dimensional accuracy of the produced part in comparison to its CAD design was checked using an automatic "feature-based registration" function and nominal-actual comparison. Analysis annotations were selected manually at areas with high deviation and colour coding was manually adjusted. The witness specimen may however be scanned according to fixed parameters as its width will always be the same, for longer samples the scan time will simply increase using multiple scans or helical scans over the length. The witness specimen may be also scanned at higher resolution than the complex part which may be used to more clearly identify flaws or events during the build which might have occurred, such as stop-start flaws.

The analysis of powder using microCT was also suggested in a standard method – mainly for qualitative views of particle shapes, extent of internal porosity, and importantly for impurities such as dense particles (contamination). Depending on the size of the powder, either 2 μm or 0.7 μm voxel size is required.

In this round robin test, all analysis was performed at the same location by the authors of this paper. Samples submitted were from 5 different facilities. The participant names are not supplied in this paper, therefore sample numbers are used only. This anonymity is due to the wide variety of factors that can cause defects in additive manufacturing, many of which are not controlled by the vendors of systems or the operators of systems. This is in fact why quality control is so important to improve this and better understand the major causes of defect formation. All participants supplied the best possible part quality, using standard optimized process parameters, in many cases these parameters are vendor-specific and "closed" so that users are not directly aware of these values. Some participants provided more than one set of samples, due to parameter variations and hence intentionally not-optimized parameters. Table 2 summarizes the submitted samples, the goal of the parts in each case and the obtained results, which are also described in the next sections in more detail. Each participant producing a set of samples (cube, witness specimen and bracket) has a number associated with it. Two participants provided more than one set of samples and letters are used to distinguish these. Due to the anonymity of the participants, and the lack of available information on fixed vendor-specific optimized parameter sets, more details on laser spot size, hatch spacing, laser power and scan speed cannot be provided here. Some additional information which may be provided and may affect the obtained results obtained by participant 3 is the use of custom powder (all others used commercial powder), which was gas atomized at TLS using the electrode inert gas atomization (EIGA) process using user-supplied Ti6Al4V bar. The powders obtained were sieved and the 20–60 μm fraction used for this work. This powder fraction failed a standard flowability test, which will affect the even spread of powder in the build. Participant 3 also used no stress-relief heat treatment prior to removal from baseplate with a bandsaw.

3. Results and discussion

Results are presented comparatively to demonstrate the differences visually using microCT images (2D slices and 3D renderings), with quantitative values provided in tables. Each type of analysis is presented and discussed in separate sections below.

3.1. Cube porosity

The 10 mm cube analysis for porosity provides a % value for the detected porosity (in this case the minimum detectable pore width was selected as 2 voxels, i.e. 30 μm). All pores larger than 30 μm were therefore quantified and further information in the form of pore size distributions, number of pores, largest pore size, pore shape (sphericity, roundness) and distances from the surface or from the nearest next pore are available, amongst other parameters. Selected images and quantitative results are presented below in Fig. 2 and Table 3, with videos for each cube in the supplementary material. Sample 1b did not contain a 10 mm cube as this sample was produced only for the purpose of creating an intentional layered defect in the witness specimen.

The 3D porosity distributions demonstrate that despite the low average levels of porosity as shown in Table 3, their 3D locations (distributions) vary significantly and are caused by different pore/defect formation processes. Based on discussion with the participants, the results can be attributed to different processing conditions, as described below. Samples 1a,b had minimal porosity with a homogenous spread of pores across the part, this indicates good process parameters and build conditions. The pores found along vertical walls of cube samples (samples 2a,b and 3 in particular) may be explained by a contour scanning error, possibly due to gaps between the contouring tracks and the filling tracks. In the case of participant 3, this may be exaggerated due to the poor flowability of the powder as discussed in the

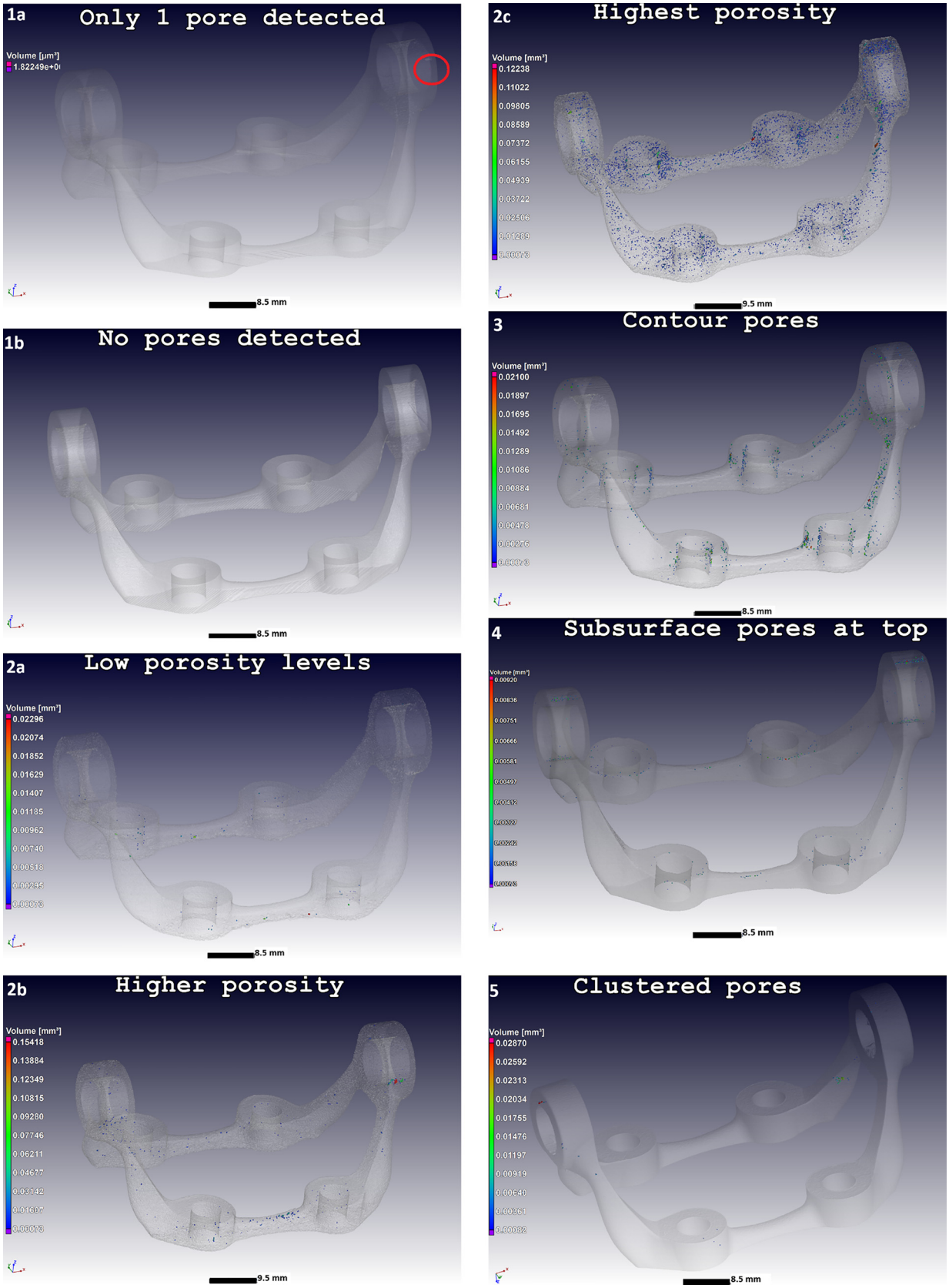

Fig. 5. Porosity analysis of brackets shown in 3D with sample numbers indicated, significantly varying distributions and amounts of porosity are identified and indicated. Supplementary videos are available for samples 3,4 and 5 as these show particularly interesting characteristic porosity distributions, which are better visualized in a video format.

Table 6
Summary of bracket porosity.

Sample Name	Porosity %	Largest pore (mm)	Number of pores
1a	0.000	0.25	1
1b	0.000	0.00	0
2a	0.004	0.58	81
2b	0.023	1.88	300
2c	0.282	1.64	4563
3	0.056	0.75	1072
4	0.012	0.44	374
5	0.00029	0.58	32

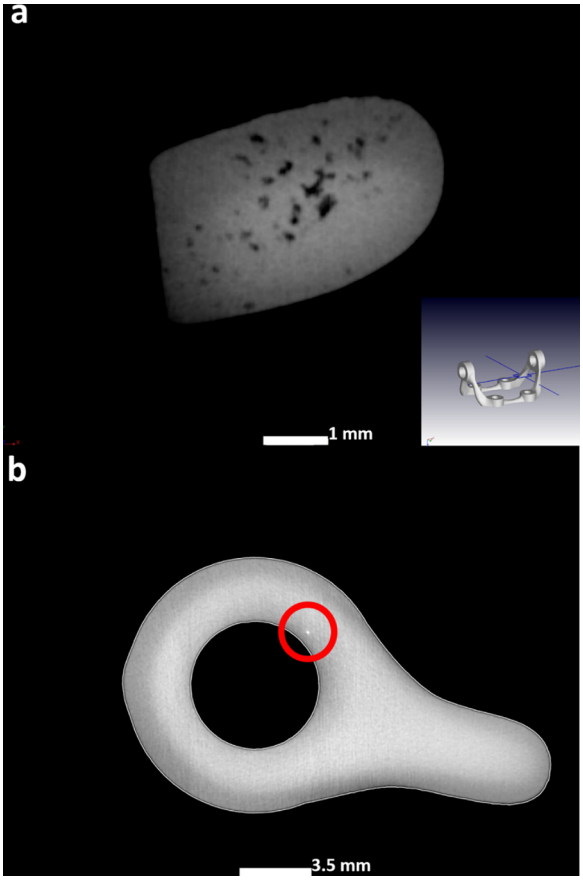

Fig. 6. Two types of defects found in sample 5 (a) clustered and layered porosity viewed here from the top in the plane of the powder bed, possibly due to improper powder delivery (black dots are pores and location of slice is shown in the 3D view to the right), and (b) a dense inclusion due to contamination of PBF system (inclusion is white spot circled in red).

methodology section. The pores along the top surface of sample 4 may be due to processing conditions varying near the top surface, optimized for surface finish rather than density. In particular, the spherical nature of these pores indicate that keyhole mode porosity was formed due to increased laser power on the final layers. The evenly distributed but relatively high porosity in sample 2c may be attributed to lack of fusion as unconsolidated powder is seen inside large pore spaces – this has been discussed in more detail in [9]. Sample 5 showed lowest porosity values but significant amounts of dense inclusions were detected which could not be quantitatively analysed due to the streak artefacts induced. These could also be obscuring some pores resulting in a false value for porosity analysis. Images of the inclusions are shown in Fig. 3. These have been identified as tungsten particles from contamination in the chamber from a previous build. The powder submitted and analysed did not show any dense particles, indicating clean feedstock as expected, indirectly confirming the chamber contamination.

3.2. Cube density

The accurate edge determination of the cubes allowed the measurement of volume from microCT data. The cubes were also weighed on a laboratory scale, providing mean density values as shown in Table 4.

These results generally are all within an acceptable range for Ti6Al4V. The density of samples 2a–c decrease with increasing porosity as expected. The advantage of this measurement is that it would identify incorrect alloy content without the need for chemical analysis, and the data is already available from the microCT scan done for its porosity analysis. It can also identify major open porosity and allow easy calculation of open/closed porosity where applicable. In this case no alloy errors were identified, no major open porosity was found, and the inclusions found in sample 5 were present in too low quantities to be detected by the mean density value.

3.3. Cube surface roughness

The method used in this study was to select a square area on one vertical wall of the cube data, and apply the methodology described in [20]. The images are shown in Fig. 4 indicating clear differences between various samples in this round robin test – quantitative results are presented in Table 5. The images are scaled to the maximum deviations as seen in the colour bars, showing that maximum deviations in sample 1a is 0.1 mm, in samples 2 approximately 0.2 mm and in samples 3,4and 5 roughly 0.05 mm. The roughest samples are therefore samples 2, with sample 1 being an intermediate roughness. Samples 3–5 show similar roughness images with slight differences in texture. The measurement method makes use of absolute maximum deviation values for the surface data relative to a mean plane at every point in a square area. This allows calculation of Sa values as reported in Table 5.

The measurement of surface roughness is a topic of much current interest, there has even been a recent interlaboratory metrology test focusing on surface roughness and dimensional accuracy of the CT systems used [32]. The same authors also demonstrated recently some correlation between surface features and internal defects as shown in [33]. In this work the single track width was correlated with internal defect formation. It can be understood that under certain conditions, the surface roughness due to laser and scan parameters will result in certain defect formation regimes, as discussed in more detail in [9]. In the results presented here, participant 4 had a particularly good surface roughness value on side walls and an exceptional surface quality of the top surface (not measured). However, this top surface had significant subsurface spherical porosity as shown in the previous section. This porosity is explained by keyhole-mode pore formation, by increasing the laser power on the final finishing layers, aimed at improving surface finish. This further motivates the need for internal detailed porosity analysis for process parameter optimization, and indicates that a smooth surface is not always associated with low porosity.

3.4. Dimensional accuracy and porosity of bracket

The bracket sample was analysed using a typical microCT analysis workflow, but this is not fully standardized as scan parameters depend on part size (a larger part might require different settings). In this case the process is similar to that used for the cube as described in the methodology section, with a different voxel size and different current setting. For a larger part, these will again need to be modified. The image analysis is identical to the cube, in order to obtain a good surface determination on the edge of the bracket, and obtain porosity results. In addition, the CAD model is imported and a feature-based registration used to overlap the CAD model and the microCT data of the bracket. This is used to make a CAD variance analysis, i.e. a geometric accuracy

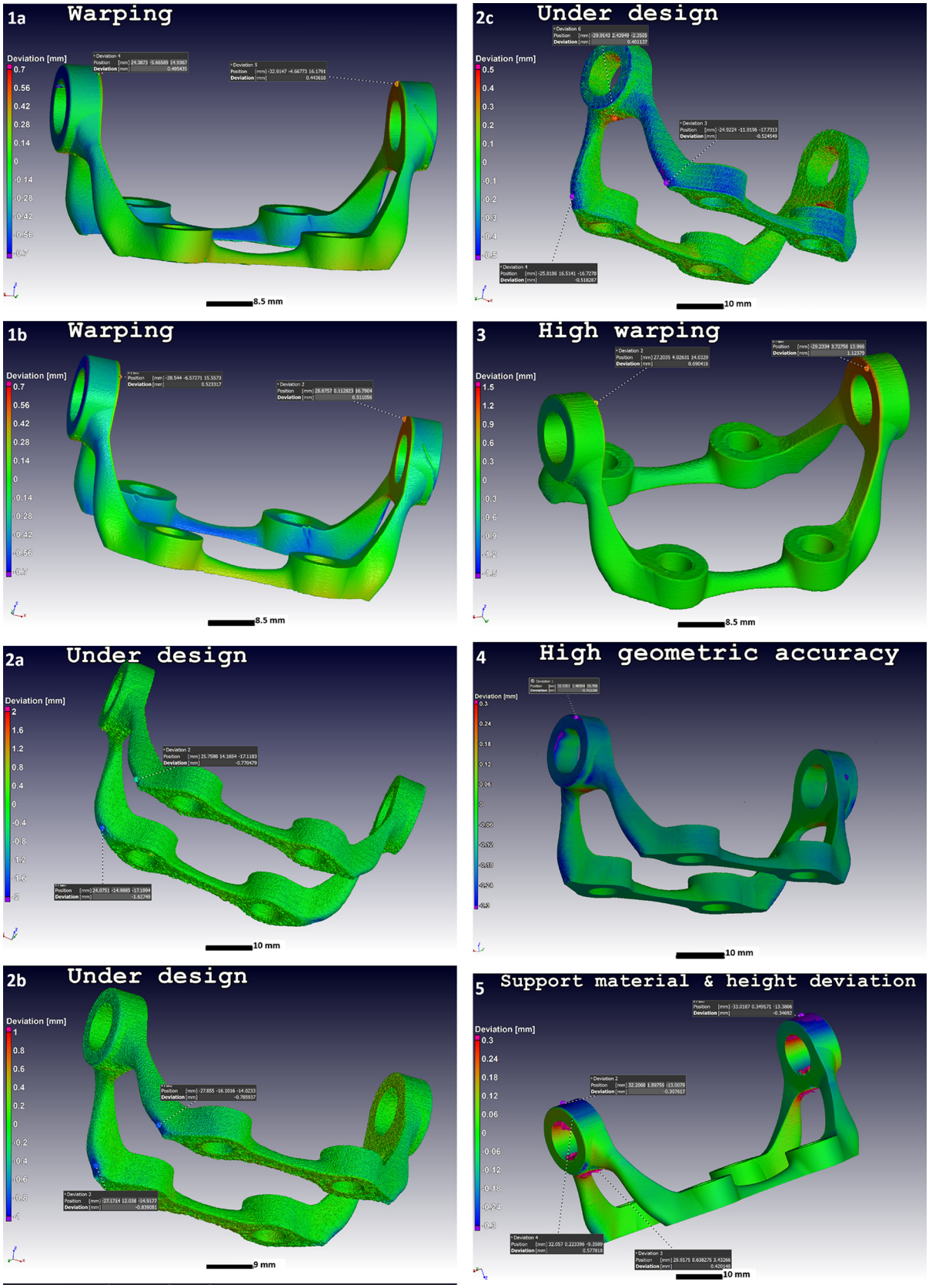

Fig. 7. Dimensional accuracy using a CAD variance analysis and identification of largest deviations using annotations.

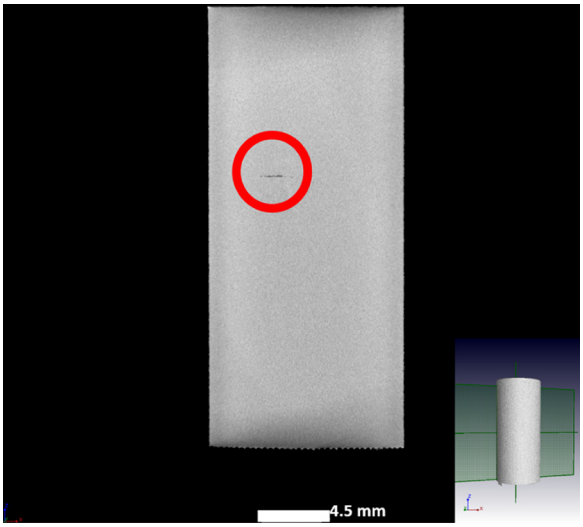

Fig. 8. Witness specimen CT slice view showing layered stop-start flaw in sample 1b (black horizontal line).

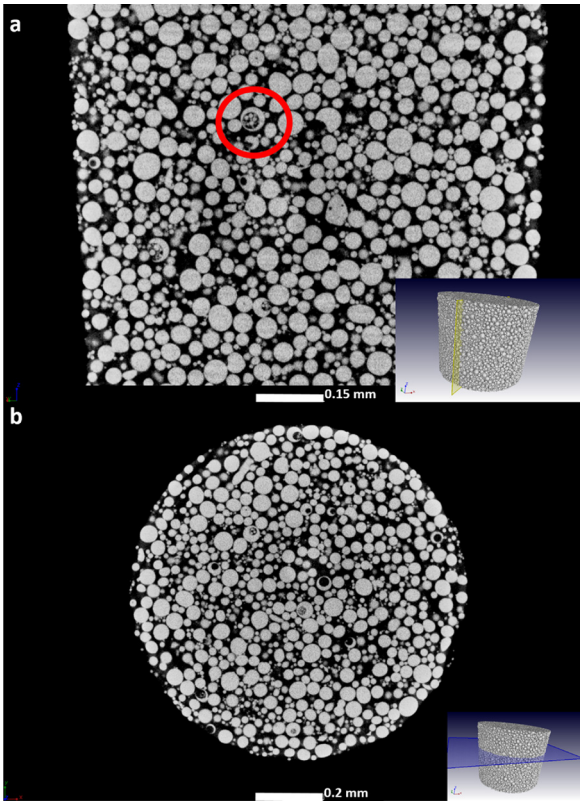

Fig. 9. Powder microCT analysis of powder from participant 3 – showing typical gas atomization porosity in some particles but also some pores filled with fine powders.

assessment.

In this case the interest was to demonstrate that (i) the different porosity distributions largely do indeed transfer to the complex part, with sometimes additional porosity/flaws incorporated due to the complex shape or other factors during the build, and (ii)the geometric accuracy may also vary and might be also associated with different processing conditions. Results are shown in Fig. 5 in 3D with pores colour-coded according to size, similar to that in Fig. 2.

The results in Fig. 5 and Table 6 indicate significantly varying porosity distributions in the brackets. The minimum detectable pore in this scan setup using voxel size 45 µm is 90 µm. The sample 1a contains only one detected pore and 1b none at all in this size range. Samples 2a–c show progressively increasing porosity, following the same trend as its cube samples. This indicates the major influence of process parameters on the porosity distribution and confirms the transfer of porosity in cube samples to larger more complex parts. Sample 3 showed most of its pores around vertical walls (near the edges) similar to its cube sample, again explained by its contouring error identified in the associated cube sample, also showing the transfer of this type of porosity to complex part. Sample 4 showed an interesting porosity distribution all along the top surface but clearly under-surface by approximately 0.4 mm (and an extremely smooth surface so no influence of surface roughness associated with it). This also follows the same trend as its cube sample, with the exception that less porosity is found along curved upwards-facing surfaces – the most is found along specifically horizontal top surfaces. Sample 5 shows very low mean porosity similar to its cube sample, but some clustering is found in layers in the build plane, for these pores, in different layers. This may be attributed to improper powder scraping. For high density parts to be produced, the powder bed needs to be level and an even spread of powder must be delivered on each layer by a scraper. It can be understood that when this is not the case, for example when an uneven powder is exposed to the focused laser beam travelling at high speed, irregularies may occur and unmelted areas may result. In this case the most likely cause of the clustered and layered porosity seen is an uneven spread of powder, either caused by a damaged scraper, lack of powder flowability due to irregularities in the powder or other causes. The clustered layered pores found in sample 5 are shown in more detail in slice image in Fig. 6a and in the supplementary video material. In addition this sample also contains isolated inclusion particles similar to its cube, also shown in Fig. 6b.

Dimensional accuracy was checked against the CAD model design and deviations from design highlighted with annotations indicating the maximum deviations at particular points, as shown in Fig. 7 for each part produced. The results shown in Fig. 7 show various issues, the most important of which is the warping of the vertical parts of the bracket towards each other by 1 mm on either side in sample 3. All samples have some form of dimensional inaccuracy but in all cases < 1 mm, and in most cases less than 0.3 mm. The acceptability of these values might depend on the criticality or dimensional tolerance of the application, but the focus here is to highlight differences from this round robin test only and not make statements about acceptability. Geometrical inaccuracies are from warping inwards on the vertical arms in samples 1a,b and sample 3. Samples 2a,b,c all show an area where too little material was built (under design). Sample 4 shows the best geometric accuracy in this test but one small area were material is missing. Sample 5 shows some support material on the down-skin sections but also the entire model is build with an inaccuracy in the z-direction, i.e. it is not the correct height as designed.

3.5. Witness specimen rods

The witness specimens were all analysed for possible layered porosity distributions. In this work one intentional layered defect was produced (1b), by stopping the AM system for a few hours and then restarting it. This is an extreme scenario, which results in the already built part to cool down and shrink, the next layer of powder is then thicker than the rest of the layers causing a partially unmelted layered flaw. It is currently thought that this represents a typical layered flaw which can also be caused by a sudden drop in laser powder, also causing imperfect melting in a single layer, or due to imperfect powder spreading as mentioned in the previous sections. The intentional layered defect was found in this sample but not in the associated bracket built alongside it, despite high resolution scans of potential areas in the bracket. The layered defect in 1b is shown in a slice image in Fig. 8 as a black horizontal line (circled in red). Other witness

specimen samples showed no unexpected flaws and are therefore not shown here.

3.6. Powder

Powder analysis was not performed for all participants, since not all participants supplied powder. However, the results of participant 3 were further investigated and the powder used was found to have poor flowability as mentioned previously. This powder was microCT scanned according to the method [22] at 0.7 µm, showing particles with internal pores filled with finer powder particles (Fig. 9). This might result in fine powders passing the sieving process hidden in partially open particles, escaping later when flowability is tested or when used in the system. Powder with too small sizes is known to reduce the flowability properties. This requires further investigation but is added here to demonstrate the ability to detect issues with powder quality, which might correlate to final build quality.

4. Conclusions

Newly developed standardized test procedures were applied to quantitatively analyse Ti6Al4V parts from different AM systems allowing direct comparison and identification of different types of intentional and unintentional flaws. Detailed porosity information from 10 mm cubes provided insight into the process parameters indicating potential for improvement in some cases. These porosity distributions largely extend into the complex part (bracket) as well. In addition the complexity of the bracket leads to larger unintentional pores in places. A layered stop-start flaw was induced intentionally and positively identified in a witness specimen, but not in the complex part associated with it. Layered flaws, most likely due to imperfect powder delivery were identified in a bracket from a different system as well (sample nr 5). One unexpected and novel result is the observation of fine powder found inside pores inside larger powder particles (participant 3).

The results of this round robin test are clearly useful as a guideline for improvement of AM processes and quality control in AM. The results show that various imperfections can be easily identified and used for improvement of processes. Since all work here involved one microCT facility, the next step involves selecting one representative set of parts from this batch and performing a reverse round robin test. This reverse test is currently underway and involves various microCT facilities, to investigate the reproducibility of the standardized methods and highlight differences in analysis that might be found, and how to modify the analysis for these cases, and thereby improve the confidence in the results typically obtained from microCT, making the technique more accessible as a routine technique for quality inspection in additive manuafacturing.

Acknowledgements

All participants in this round robin test are gratefully acknowledged for their support in this effort. The South African Department of Science and Technology through the CPAM program is acknowledged for its support of this project.

Appendix A. Supplementary data

Supplementary material related to this article can be found, in the online version, at doi:https://doi.org/10.1016/j.addma.2018.09.014.

References

[1] M. Schmidt, M. Merklein, D. Bourell, D. Dimitrov, T. Hausotte, K. Wegener, L. Overmeyer, F. Vollertsen, G.N. Levy, Laser based additive manufacturing in industry and academia, CIRP Ann. 66 (2017) 561–583, https://doi.org/10.1016/J.CIRP.2017.05.011.

[2] T. Debroy, H.L. Wei, J.S. Zuback, T. Mukherjee, J.W. Elmer, J.O. Milewski, A.M. Beese, A. Wilson-Heid, A. De, W. Zhang, Additive manufacturing of metallic components—process, structure and properties, Prog. Mater. Sci. 92 (2018) 112–224, https://doi.org/10.1016/j.pmatsci.2017.10.001.

[3] I. Yadroitsev, P. Krakhmalev, I. Yadroitsava, A. Du Plessis, Qualification of Ti6Al4V ELI alloy produced by laser powder bed fusion for biomedical applications, JOM 70 (2018) 372–377, https://doi.org/10.1007/s11837-017-2655-5.

[4] M. Qian, W. Xu, M. Brandt, H.P. Tang, Additive manufacturing and postprocessing of Ti-6Al-4V for superior mechanical properties, MRS Bull. 41 (2016) 775–784, https://doi.org/10.1557/mrs.2016.215.

[5] M. Seifi, A. Salem, J. Beuth, O. Harrysson, J.J. Lewandowski, Overview of materials qualification needs for metal additive manufacturing, JOM 68 (2016) 747–764, https://doi.org/10.1007/s11837-015-1810-0.

[6] M. Seifi, M. Gorelik, J. Waller, N. Hrabe, N. Shamsaei, S. Daniewicz, J.J. Lewandowski, Progress towards metal additive manufacturing standardization to support qualification and certification, JOM 69 (2017) 439–455, https://doi.org/10.1007/s11837-017-2265-2.

[7] Q.Y. Lu, C.H. Wong, Applications of non-destructive testing techniques for post-process control of additively manufactured parts, Virtual Phys. Prototyp. 12 (2017) 301–321, https://doi.org/10.1080/17452759.2017.1357319.

[8] J.A. Slotwinski, E.J. Garboczi, K.M. Hebenstreit, Porosity measurements and analysis for metal additive manufacturing process control, J. Res. Inst. Stand. Technol. 119 (2014) 494–528, https://doi.org/10.6028/jres.119.019.

[9] A. du Plessis, I. Yadroitsev, I. Yadroitsava, S.G. Le Roux, X-ray microcomputed tomography in additive manufacturing: a review of the current technology and applications, 3D Print. Addit. Manuf. 0 (2018), https://doi.org/10.1089/3dp.2018.0060.

[10] A. du Plessis, S.G. le Roux, F. Steyn, X-ray computed tomography of consumer-grade 3D-printed parts, 3D Print. Addit. Manuf. 2 (2015) 190–195, https://doi.org/10.1089/3dp.2015.0015.

[11] A. Du Plessis, S.G. Le Roux, F. Steyn, Quality investigation of 3D printer filament using laboratory X-ray tomography, 3D Print. Addit. Manuf. 3 (2016) 262–267, https://doi.org/10.1089/3dp.2016.0011.

[12] G.D. Goh, V. Dikshit, A.P. Nagalingam, G.L. Goh, S. Agarwala, S.L. Sing, J. Wei, W.Y. Yeong, Characterization of mechanical properties and fracture mode of additively manufactured carbon fiber and glass fiber reinforced thermoplastics, Mater. Des. 137 (2018) 79–89, https://doi.org/10.1016/j.matdes.2017.10.021.

[13] S. Agarwala, G.L. Goh, Y.L. Yap, G.D. Goh, H. Yu, W.Y. Yeong, T. Tran, Development of bendable strain sensor with embedded microchannels using 3D printing, Sens. Actuators A: Phys. 263 (2017) 593–599, https://doi.org/10.1016/j.sna.2017.07.025.

[14] A. Du Plessis, S.G. Le Roux, G. Booysen, J. Els, Quality control of a laser additive manufactured medical implant by X-Ray tomography, 3D Print. Addit. Manuf. 3 (2016) 175–182, https://doi.org/10.1089/3dp.2016.0012.

[15] ASTM E1570-11, Standard Practice for Computed Tomographic (CT) Examination, ASTM E1570-11, (2011).

[16] ASTM WK56649, Standard Practice/Guide for Intentionally Seeding Flaws in Additively Manufactured (AM) Parts, (2018).

[17] ASTM WK47031, Standard Guide for Post-Process Non-destructive Testing of Metal Additively Manufactured Parts Used in Aerospace Applications, (2018).

[18] A. du Plessis, Standard Method for microCT-Based Additive Manufacturing Quality Control 1: Porosity Analysis, Protocols.IO, (2018) https://www.protocols.io/view/standard-method-for-microct-based-additive-manufac-sc7eazn?abstract.

[19] A. du Plessis, Standard Method for microCT-Based Additive Manufacturing Quality Control 2: Density Measurement, Protocols.IO, (2018) https://www.protocols.io/view/standard-method-for-microct-based-additive-manufac-sbvean6.

[20] A. du Plessis, Standard Method for microCT-Based Additive Manufacturing Quality Control 3: Surface Roughness, Protocols.IO, (2018) https://www.protocols.io/view/standard-method-for-microct-based-additive-manufac-sbweape.

[21] A. du Plessis, Standard Method for microCT-Based Additive Manufacturing Quality Control 5: Witness Specimen, Protocols.IO, (2018) https://www.protocols.io/view/standard-method-for-microct-based-additive-manufac-sbzeap6.

[22] A. du Plessis, Standard Method for microCT-Based Additive Manufacturing Quality Control 4: Powder Characterization, Protocols.IO, (2018) https://www.protocols.io/view/standard-method-for-microct-based-additive-manufac-sbyeapw.

[23] G. Pyka, G. Kerckhofs, I. Papantoniou, M. Speirs, J. Schrooten, M. Wevers, Surface roughness and morphology customization of additive manufactured open porous Ti6Al4V structures, Materials (Basel) 6 (2013) 4737–4757, https://doi.org/10.3390/ma6104737.

[24] G. Kerckhofs, G. Pyka, M. Moesen, S. Van Bael, J. Schrooten, M. Wevers, High-resolution microfocus X-ray computed tomography for 3D surface roughness measurements of additive manufactured porous materials, Adv. Eng. Mater. 15 (2013) 153–158, https://doi.org/10.1002/adem.201200156.

[25] A. Thompson, N. Senin, C. Giusca, R. Leach, Topography of selectively laser melted surfaces: a comparison of different measurement methods, CIRP Ann. Manuf. Technol. 66 (2017) 543–546, https://doi.org/10.1016/J.CIRP.2017.04.075.

[26] A. Thompson, N. Senin, I. Maskery, L. Körner, S. Lawes, R. Leach, Internal surface measurement of metal powder bed fusion parts, Addit. Manuf. 20 (2018) 126–133, https://doi.org/10.1016/j.addma.2018.01.003.

[27] K. Heim, F. Bernier, R. Pelletier, L.-P. Lefebvre, High resolution pore size analysis in metallic powders by X-ray tomography, Case Stud. Nondestruct. Test. Eval. 6 (2016) 45–52, https://doi.org/10.1016/J.CSNDT.2016.09.002.

[28] C. Rothleitner, U. Neuschaefer-Rube, J. Illemann, Size and shape determination of sub-millimeter sized abrasive particles with X-ray computed tomography, 6th Conf. Ind. Comput. Tomogr. (2016), pp. 1–9 (Accessed 20 February 2018), www.3dct.at.

[29] F. Bernier, R. Tahara, M. Gendron, Additive manufacturing powder feedstock

characterization using X-ray tomography, Met. Powder Rep. 73 (2018) 158–162, https://doi.org/10.1016/j.mprp.2018.01.002.
[30] A. du Plessis, C. Broeckhoven, A. Guelpa, S.G. le Roux, Laboratory x-ray micro-computed tomography: a user guideline for biological samples, Gigascience 6 (2017) 42–49, https://doi.org/10.1093/gigascience/gix027.
[31] A. du Plessis, S.G. le Roux, A. Guelpa, The CT scanner facility at Stellenbosch University: an open access X-ray computed tomography laboratory, Nucl. Instrum. Methods Phys. Res. Sect. B: Beam Interact. Mater. Atoms 384 (2016) 42–49, https://doi.org/10.1016/j.nimb.2016.08.005.
[32] A. Townsend, R. Racasan, R. Leach, N. Senin, A. Thompson, A. Ramsey, D. Bate, P. Woolliams, S. Brown, L. Blunt, An interlaboratory comparison of X-ray computed tomography measurement for texture and dimensional characterisation of additively manufactured parts, Addit. Manuf. 23 (2018) 422–432, https://doi.org/10.1016/j.addma.2018.08.013.
[33] A. Thompson, S. Tammas-williams, N. Senin, I. Todd, M.M. Team, Correlating Volume and Surface Features in Additively Manufactured Metal Parts 1 Manufacturing Metrology Team, Faculty of Engineering, 2 Manufacture using Advanced Powder Processes (MAPP), ePrints Nottingham (2018) 1–5.